This is the peer reviewed version of the following article: [Toru Kanahashi, Shigehito Yamada, Akio Yoneyama, Tetsuya Takakuwa. (2019), Relationship Between Physiological Umbilical Herniation and Liver Morphogenesis During the Human Embryonic Period: A Morphological and Morphometric Study. Anat Rec (Hoboken). 2019 Nov;302(11):1968-1976. doi: 10.1002/ar.24149. Epub 2019 May 29], which has been published in final form at DOI: https://doi.org/10.1002/ar.24149. This article may be used for non-commercial purposes in accordance with Wiley Terms and Conditions for Use of Self-Archived Versions.

Relationship Between Physiological Umbilical Herniation and Liver Morphogenesis During the Human Embryonic Period: A Morphological and Morphometric Study

Toru Kanahashi[1], Shigehito Yamada[1,2], Akio Yoneyama[3], Tetsuya Takakuwa[1]

[1]Human Health Science, Graduate School of Medicine, Kyoto University, Kyoto 606-8507, Japan

[2]Congenital Anomaly Research Center, Graduate School of Medicine, Kyoto University, Kyoto 606-8501, Japan

[3]The Kyushu Synchrotron Light Research Center, Saga 841-0005, Japan

Corresponding author:

Dr. Tetsuya Takakuwa

Human Health Science, Graduate School of Medicine, Kyoto University

606-8507 Sakyo-ku Shogoin Kawahara-cyo 53, Kyoto, Japan

TEL/FAX: +81-75-751-3931; E-mail: tez@hs.med.kyoto-u.ac.jp

Running title: PUH and liver morphogenesis

Grant sponsor: Japan Society for the Promotion of Science;
Grant numbers: 26220004, 16K15535, 17H05294, and 18K07876.

Abstract

It is widely hypothesized that physiological umbilical herniation (PUH) in humans occurs because the liver occupies a large space in the abdominal cavity, which pushes the intestine into the extra-embryonic coelom during the embryonic period. We have recently shown the presence of the intestinal loop in the extra-embryonic coelom in embryos with liver malformation. Here, we analyzed the relationship between the liver and PUH at Carnegie stage 21 of four embryos with liver malformation, including two with hypogenesis (HY1, HY2) and two with agenesis (AG1, AG2), using phase-contrast X-ray computed tomography and compared them to two control embryos. The intestinal loop morphology in the malformed embryos differed from that in the control embryos, except in HY1. The length of the digestive tract in the extra-embryonic coelom of the embryos with liver malformation was similar or longer than that of the controls. The rate of intestinal loop lengthening in the extraembryonic coelom compared to that of the total digestive tract in all embryos with liver malformation was similar or higher than that of the controls. The estimated total abdominal cavity volume in the embryos with liver malformation was considerably smaller than that of the controls, while the intestinal volume was similar. The cardia and proximal portion of the pancreas connecting to the duodenum were located at almost identical positions in all the embryos whereas other parts of the upper digestive tract deviated in the embryos with abnormal livers. Thus, our results provided evidence that PUH occurred independently of liver volume.

Key words: Physiological umbilical herniation, Liver morphogenesis, Liver malformation, Total abdominal cavity volume, Intestinal volume.

Introduction

The human intestine lengthens much more rapidly during the embryonic period (Meckel, 1817) and develops a dorsoventral hairpin fold called the primary intestinal loop at the Carnegie stage (CS) 14 (Kim et al., 2003). The intestine temporarily distributes in both the abdominal coelom and extra embryonic coelom in the umbilicus. Such a condition was classically referred to as physiological umbilical herniation (PUH) (Meckel, 1817; Mall, 1898). A previous study showed that PUH begins from CS 17 (Ueda et al, 2016), and is followed by reduction in which the intestine returns to the abdominal coelom during the early-fetal period (Kim et al., 2003). Finally, the intestine assumes its adult position by fixation of the mesentery. During these processes, the intestine is hypothesized to undergo a counterclockwise rotation of 270°.

Mall (1899) advocated the most simple and probable cause of PUH as the liver growing very rapidly and almost entirely filling the abdominal cavity. As a result, it pushes the intestine into the extra-embryonic coelom. Recent textbooks present descriptions consistent with Mall's theorem (Gary et al., 2009; Moore et al., 2008). However, ever since Mall's description was put forth, no data indicating the actual mechanism of PUH have been reported.

We have recently shown human embryonic samples at CS 21 with liver malformation in which the intestinal loop is within the extra-embryonic coelom (Kanahashi et al., 2016). We doubted Mall's description because the intestinal loop was even within the extra-embryonic coelom of embryos with hypogenetic and agenetic livers. Detailed analyses of these embryos may be valuable for reconsidering the mechanism of PUH, which could occur due to reasons other than the growth and occupation of the liver in the abdominal cavity. Thus, in the current study we aimed to examine the precise relationship between the liver and PUH using both morphological and morphometric approaches by comparing embryos with liver hypogenesis, liver agenesis, and normal liver. Herein, we discuss the mechanisms underlying the occurrence of PUH.

Materials & Methods

Human embryo specimens

Approximately 44,000 human embryos comprising the Kyoto Collection of Human Embryos are currently stored at the Congenital Anomaly Research Center of Kyoto University (Nishimura et al., 1968; Yamada et al., 2006; Shiota et al., 2007). Most of the embryos were obtained after pregnancy termination during the first trimester for socioeconomic reasons under the Maternity Protection Law of Japan. The current study was approved by the ethics committee of the Kyoto University Graduate School and Faculty of Medicine (E986), In the laboratory, the aborted embryos were measured, examined, and staged using the criteria for Carnegie staging described by O'Rahilly and Müller (1987), which is used internationally (Moore, 2008). Staging was based on the external and internal morphological development of the embryo, independent of both age and size.

Four embryos consisting of two embryos with liver hypogenesis (HY1, HY2) and two embryos with liver agenesis (AG1, AG2), as well as two control embryos, all at CS 21, were used in the study. These embryos were selected and described in part for our previous study (Kanahashi et al, 2016). Briefly, 1,156 magnetic resonance imaging (MRI) datasets at CS 14 to CS 23 were selected from the Kyoto collection as externally normal embryos (Matsuda et al., 2003; Shiota et al., 2007; Yamada et al., 2010). The 1,156 embryos were screened using liver volume as the target organ. Embryos with liver volumes 2 standard deviations above or below the mean for the stage of development were selected and examined using MRI. Embryos identified with potentially abnormal livers were further analyzed by using phase-contrast X-ray computed tomography (PXCT). Complications in the organs other than the liver are summarized in Table 1. Four embryos with liver anomaly showed defects partly at the outside of umbilical cord (e.g. Wharton's Jelly), while the digestive tract, umbilical arteries, vein, and proximal part of the umbilicus and abdominal wall remained intact. The two control embryos were normal, both externally and with respect to liver morphology. The previous study elucidated that the prevalence of

liver malformations in CS18 and CS21 in the intrauterine population of externally normal embryos is approximately 1.7% (Kanahashi et al, 2016). Most of such liver abnormality embryos do not survive because liver function becomes essential (Koga, 1971; Migliaccio et al., 1986; Tavian et al., 1999).

Acquisition of 3D images with PXCT

The 3-D PXCT images of the human embryos were obtained using a radiographic imaging system (BL14-C, 17.8 keV) from Photon Factory, Institute of Materials Structure Science, High Energy Accelerator Research Organization (KEK, Tsukuba, Japan). The data provided a resolution of 18 μm/pixel. The mechanism and conditions used to acquire the PXCT images of embryos have been described elsewhere (Yoneyama et al., 2011).

Image analysis and morphometry

The structures of the digestive tract, including the esophagus, stomach, duodenum, intestinal loop, and colorectum, were reconstructed for each image set using the Amira software suite (version 5.5.0; Visage Imaging, Berlin, Germany). The length of the digestive tract was measured as described previously (Ueda et al., 2016). Briefly, the AmiraSkel software module was used to determine the centerline length of the digestive tract. The lengths of the total digestive tract (Total length) were set from the pyloric sphincter to the end of the intestinal loop. Since the end of the intestinal loop may correspond to the point at which the length of the mesentery drastically changes, as described by Soffers et al. (2015), it was defined in the current study as the most obvious dorsal inflection point on the 3D image. The length of intestinal loop in the extraembryonic coelom (extra length) was measured in the 3-D image from the point where the intestinal loop first entered the extraembryonic coelom to the last point of return to the abdominal coelom. The estimated total abdominal cavity volume and liver volume were measured by manual segmentation of the transverse section on sequential 2-D images using the Amira software. For the

total abdominal cavity volume, the slices including the cranial end of the diaphragm through the lower pole of the metanephros were used. The estimated intestinal volume was calculated by subtracting the liver volume from the estimated total abdominal cavity volume.

Results

Morphological features of the intestinal loop

The digestive tracts, livers, and other intra-abdominal organs were clearly detectable in the PXCT images of all embryos (Fig. 1). No internal damage was detected in any of the embryos. The elongated intestines entered the extra-embryonic coelom in all the embryos examined, both in the controls and in the embryos with liver hypogenesis or agenesis (Figs. 1 and 2).

The cecum was located to the left of the superior mesenteric artery (SMA) in the controls and in all malformed embryos except AG1 in which the cecum was located close to tip of the intestinal loop (Fig. 1). The intestinal loop had a secondary loop in the extra-embryonic coelom (Figs. 1 and 2). The number of secondary loops was the same in all embryos except HY2, which showed a greater number of secondary loops compared to that in the controls (Table 1, Fig. 2).

The proximal part of the intestinal loop ran straight across at the border between the abdominal coelom and extra-embryonic coelom in the two control embryos and AG1 (see red circle in Fig. 1 and red dashed line in Fig. 2). The secondary loop was located on the border between the abdominal coelom and extra-embryonic coelom in HY1, HY2, and AG2. The distal part from the cecum of the intestinal loop, which is equivalent to the large intestine, ran straight across the border between the abdominal coelom and the extra-embryonic coelom in all embryos except AG2 in which the intestinal tract from the cecum to the colorectum was not recognized (see * in Fig. 2).

Length measurements of the digestive tract

The Total length (a) and extra length (b) were measured (Fig. 3A) and the b/a ratio was calculated (Fig. 3B, Table 1). The Total length in control 1 and control 2 was 29 mm and 26 mm (mean 28 mm), respectively. In HY1 and HY2, the Total length was similar to that of the controls or longer (HY1, 27 mm; HY2, 33 mm). In AG1 and AG2, the Total length was shorter than that of the controls (AG1, 23 mm; AG2, 21 mm).

The extra length in control 1 and control 2 was 20 mm and 17 mm, respectively, with a mean of 19 mm. In HY1 and HY2, the extra length was longer than that of the controls (HY1, 23 mm; HY2, 22 mm). In AG1 and AG2, the extra length was similar to that of the controls (AG1, 19 mm; AG2, 18 mm).

The ratios of extra length to Total length in the controls were 69% and 65% (mean 67%). In HY1 and HY2, the ratios of extra length to Total length were similar to or higher than those in the controls (HY1, 84 %; HY2, 67 %). In AG1 and AG2, the ratios of extra length to Total length were higher than those in the controls (AG1, 82%; AG2, 87%).

Estimated abdominal volume

Images of the mid-sagittal sections of the abdominal cavity and its contents of control 1, HY1, and AG1 are shown in Fig. 4A. The liver and digestive tract occupied almost the entire abdominal space. The liver occupied the dominant amount of space in the controls. In contrast, the digestive tract occupied most of the abdominal space in the embryos with liver malformation.

Total estimated volumes of the abdominal cavities and intestines were calculated (Fig. 4B, Table 1). The estimated total abdominal cavity volumes in the controls were 63 mm^3 and 50 mm^3 (mean 57 mm^3). Compared to those in the controls, the estimated total abdominal cavity volumes were markedly lower in the embryos with liver malformation (HY1, 30 mm^3; HY2, 36 mm^3; AG1, 21 mm^3; and AG2, 18 mm^3). Decreased liver volumes directly contributed to the decreases observed in the estimated total abdominal cavity volumes in the embryos with malformations.

In the controls, the intestinal volumes were 24 mm^3 and 16 mm^3 with a mean of 20 mm^3. In HY1 and HY2, the intestinal volumes were consistent with those in the controls or higher (HY1, 23 mm^3; HY2, 28 mm^3). In AG1 and AG2, the intestinal volumes were consistent with those in the controls or lower (AG1, 21 mm^3; AG2, 18 mm^3).

The volumes of the bilateral adrenal glands and metanephros were also calculated. In the controls, the volumes of bilateral adrenal glands were 1.7 mm^3 and 2.0 mm^3 (mean 1.9 mm^3) and the volumes of the bilateral metanephros were 1.0 mm^3 and 0.6 mm^3 (mean 0.8 mm^3). In the embryos with liver malformation, the volumes of the bilateral adrenal glands were similar to those in the controls or at most 1.0 mm^3 higher (HY1, 2.0 mm^3; HY2, 3.0 mm^3; AG1, 2.6 mm^3; AG2, 2.1 mm^3). The volumes of bilateral metanephros in the embryos with liver malformation were almost the same as those of the controls (HY1, 1.0 mm^3; HY2, 1.0 mm^3; AG1, 0.8 mm^3; AG2, 0.8 mm^3). Morphological abnormality of the bilateral adrenal glands and metanephros in embryos with liver malformation were not detected (data not shown).

Deviation of the upper digestive tract (stomach, duodenum) and pancreas

To compare the deviation of the upper digestive tract and pancreas in embryos with liver malformation as that of controls, we evaluated reconstructed 3-D images of the digestive tract in all the embryos (Fig. 5). Two anatomical references, the cardia and proximal part of the pancreas connecting to the duodenum, were located at almost identical positions in all the embryos with liver abnormality and in the controls, indicating that no deviation developed around these two landmarks. The SMA was located just dorsal to the proximal part of the pancreas. The duodenum was connected to the posterior abdominal wall via short dorsal mesentery except at the end of the duodenum. The duodenum was directly connected to the posterior abdominal wall at the end of the duodenum (Fig. 5).

However, other regions of the upper digestive tract, such as the body of the stomach, the pylorus, the descending and horizontal parts of the duodenum, and the body and tail of the pancreas, were deviated in the embryos with liver

malformation (Table 1). In HY2, the body of the stomach deviated ventrally and cranially, the descending part of the duodenum deviated caudally, and the horizontal portion deviated ventrally (data not shown). In AG1 and AG2, the body of the stomach deviated ventrally and cranially and was thus inverted. In addition to the inversion, deformation was also observed in body of the stomach of AG1 and AG2. In the embryos with agenesis (AG1, AG2), the digestive tracts from the pyloric antrum to the upper region of the duodenum were straight and ran vertically in the right ventral quadrant. As for the pancreas, the body and tail deviated ventrally and cranially in the embryos with liver malformation. The degree of deviation was greater in the embryos with agenesis (AG1, AG2) compared to that in the embryos with hypogenesis (HY1, HY2).

Discussion

Mall (1899) proposed rapid liver growth in the abdominal space as the simplest and most probable cause of PUH. Many studies have examined intestinal loop morphology and morphometry in the digestive tract during embryonic and fetal periods (Frazer and Robbins, 1915; Dott, 1923; Snyder and Chaffin, 1952, 1954; Kim et al., 2003; Metzger et al., 2011; Soffers et al., 2015). However, other than Mall's theory, there has been no cause of PUH described. The current study demonstrated an elongated intestinal loop distributed in both the abdominal coelom and the extra-embryonic coelom of CS 21 embryos with liver malformation, as well as in control embryos with normal liver morphology. To reconsider the cause of PUH, we examined the morphology and morphometry of the digestive tracts in embryos with liver malformations and in controls and estimated the abdominal volumes.

Ueda et al (2016) first measured the rapid elongation of the intestinal loop in the human embryonic period. Primarily owing to the small intestinal part of the intestinal loop, the intestinal tract elongated rapidly over this period. Most of the intestinal loop was morphologically observed in extra embryonic coelom, though the actual length for the extra embryonic part was not measured in that study. The present study revealed the intestinal length and morphological

features of the intestinal loop in embryos with liver malformations. Total length and extra embryonic length were almost the same (21-33 mm and 17-23 mm) in all the embryos, including those with liver malformation and the controls. Furthermore, the ratio of extra length/total length was also almost same in the embryos with liver malformations. These findings indicated that the elongation of the intestinal tract as well as distribution of intestinal tract between extra coelom and abdominal coelom was independent of liver development.

Mekonen et al (2015) described the development of the ventral body wall using historical collections of embryos and fetuses. At CS 20, the dense mesenchyme below the umbilicus is still identifiable but has split ventromedially to surround the abdominal rectus muscles. They observed that the abdominal muscles, including the rectus muscles, reach the hip bone at CS 23. Thus, the structures of the abdominal wall remain immature at CS 21 and therefore the developing abdominal muscles and mesenchymal tissue may still be soft and prone to change in their form. On the other hand, the abdominal organs such as the liver grow rapidly during the embryonic development (Hirose et al., 2012; Kanahashi et al., 2016). Among the abdominal organs, the liver was the most likely to expand the abdominal wall and to increase the abdominal volume. There was less of a possibility that the abdominal organs other than the liver were responsible for the increased abdominal volume. For instance, the volumes of adrenal grands in the embryos with liver malformation were at most 1.0 mm^3 larger than that of the controls. Such an increase seemed to be small and was likely negligible. We speculate that it was primarily the liver that pushed to change the form of abdominal wall. Correspondingly, a reduction in liver volume may result in a decreased abdominal volume.

Two anatomical references, the cardia and the proximal part of the pancreas connecting to the duodenum, were located at almost identical positions in the controls and all the embryos with liver malformation, whereas the body of the stomach and the body and tail of the pancreas were deviated in the embryos with liver malformation. Deviation may be anatomically restricted in these two references. The cardia was located close to the diaphragm in all embryos. The septum transversum differentiates into the diaphragm after CS 17 (Hirose et al., 2012). Therefore, at CS 21, the movement of the cardia should be

restricted by the point at which the esophagus crosses the diaphragm. In contrast, the position of the proximal part of pancreas may be restricted by duodenum and SMA, whereas the passage of duodenum and orientation of pancreas can still be deviated to some extent. Such deviations might occur by a decrease (loss) in volume of the liver.

The present study demonstrated that the total and extra intestinal length and its ratio were almost same in all embryos irrespective of the liver volume. In contrast, a decrease in liver volume leads to a decrease in abdominal cavity volume. These findings strongly indicate that PUH occurs due to near-normal growth of the midgut and a near-normal increase in abdominal space for the midgut. Therefore, Mall's theory should be reconsidered.

Acknowledgements

We are deeply indebted to Associate Professor Kazuyuki Hyodo of Photon Factory for the use of the synchrotron radiographic equipment at BL-14C. We thank Ms. Chigako Uwabe at the Congenital Anomaly Research Center for technical assistance in handling the human embryos. We thank Dr. Tohoru Takeda at Kitasato University for acquisition of the PCXT images. This work was performed with the approval of the Photon Factory Program Advisory Committee (Proposal Nos. 2013G514, 2012G138, 2014G018, 2015G574).

Literature Cited

Dott NM. 1923. Anomalies of intestinal rotation: their embryological and surgical aspects, with report of five cases. Br J Surg 53:251-286.
Frazer JE, Robbins RH. 1915. On the factors concerned in causing rotation of the intestine in man. J Anat Physiol 50:75-110.
Gary SC, Steven BB, Philip BR, Philippa FH. 2009. Development of the gastrointestinal tract. In: Hyde M, Gruliow R, editors. Larsen's Human Embryology 4th ed. Philadelphia: Churchill Livingstone, Elsevier. p 456-457.
Hirose A, Nakashima T, Yamada S, Uwabe C, Kose K, Takakuwa T. 2012. Embryonic liver morphology and morphometry by magnetic resonance microscopic imaging. Anat Rec 295:51-59.
Kanahashi T, Yamada S, Tanaka M, Hirose A, Uwabe C, Kose K, Yoneyama A, Takeda T, Takakuwa T. 2016. A novel strategy to reveal the latent abnormalities in human embryonic stages from a large embryo collection. Anat Rec 299:8-24.
Kim WK, Kim H, Ahn DH, Kim MH, Park HW. 2003. Timetable for intestinal rotation in staged human embryos and fetuses. Birth Defects Res A Clin Mol Teratol 67:941-945.
Koga A. 1971. Morphogenesis of intrahepatic bile ducts of the human fetus. Z Anat Entwicklungsgesch 135:156-184.
Mall FP. 1898. Development of the human intestine and its position in the adult. Bull Johns Hopkins Hosp 9:197-208.
Mall FP. 1899. Supplementary note on the development of the human intestine. Anat Anz 16:492-495.
Matsuda Y, Utsuzawa S, Kurimoto T, Haishi T, Yamazaki Y, Kose K, Anno I, Marutani M. 2003. Super-parallel MR microscope. Magn Reson Med 50:183-189.
Meckel JF. 1817. Blindungsgeschichte des Darmkanals der Saugetiereund namentlich der Menschen. Deutsche Arch Physiol 3:1-84.
Mekonen HK, Hikspoors JPJM, Mommen G, Köhler SE, Lamers WH. 2015. Development of the ventral body wall in the human embryo. J Anat 227(5):673-685.
Metzger R, Metzger U, Fiegel HC, Kluth D. 2011. Embryology of the midgut. Semin Pediatr Surg 20:145-151.
Migliaccio G, Migliaccio AR, Petti S, Mavilio F, Russo G, Lazzaro D, Testa U,

Marinucci M, Peschle C. 1986. Human embryonic hemopoiesis. Kinetics of progenitors and precursors underlying the yolk sac—liver transition. J Clin Invest 78:51–60.
Moore KL, Persaud TVN, Torchia MG. 2008. The digestive system. In: Ozols I, Hyde M, DeFrancesco K, editors. The Developing Human: Clinically Oriented Embryology. Philadelphia: Sunders, Elsevier. p 224-225.
Nishimura H, Takano K, Tanimura T, Yasuda M. 1968. Normal and abnormal development of human embryos: first report of the analysis of 1,213 intact embryos. Teratology 1:281-290.
O'Rahilly R, Müller F. 1987. Developmental stages in human embryos: including a revision of Streeter's "horizons" and a survey of the Carnegie collection. Washington, D.C.: Carnegie Institution of Washington.
Shiota K, Yamada S, Nakatsu-Komatsu T, Uwabe C, Kose K, Matsuda Y, Haishi T, Mizuta S, Matsuda T. 2007. Visualization of human prenatal development by magnetic resonance imaging (MRI). Am J Med Genet A 143A:3121-3126.
Snyder WH, Jr, Chaffin L. 1952. An intermediate stage in the return of the intestines from the umbilical cord: Embryo 37 mm. Anat Rec 113:451-457.
Snyder WH, Jr, Chaffin L. 1954. Embryology and pathology of the intestinal tract: presentation of forty cases of malrotation. Ann Surg 110:368-380.
Soffers JH, Hikspoors JP, Mekonen HK, Koehler SE, Lamers WH. 2015. The growth pattern of the human intestine and its mesentery. BMC Dev Biol 15:31.
Tavian M, Hallais M, Péault B. 1999. Emergence of intraembryonic hematopoietic precursors in the pre-liver human embryo. Development 126:793–803.
Ueda Y, Yamada S, Uwabe C, Kose K, Takakuwa T. 2016. Intestinal rotation and physiological umbilical herniation during the embryonic period. Anat Rec 299:197-206.
Yamada S, Uwabe C, Nakatsu-Komatsu T, Minekura Y, Iwakura M, Motoki T, Nishimiya K, Iiyama M, Kakusho K, Minoh M, Mizuta S, Matsuda T, Matsuda Y, Haishi T, Kose K, Fujii S, Shiota K. 2006. Graphic and movie illustrations of human prenatal development and their application to embryological education based on the human embryo specimens in the Kyoto collection. Dev Dyn 235:468-477.

Yamada S, Samtani RR, Lee ES, Lockett E, Uwabe C, Shiota K, Anderson SA, Lo CW. 2010. Developmental atlas of the early first trimester human embryo. Dev Dyn 239:1585-1595.

Yoneyama A, Yamada S, Takeda T. 2011. Fine biomedical imaging using X-ray phase-sensitive technique. In: Advanced Biomedical Engineering. InTech. p 107-128.

Figure legends

Fig. 1 Three-dimensional (3-D) reconstructed PXCT images and representative 2-D images of control 1, HY1, and AG1 embryos demonstrating physiological umbilical herniation. The red circle indicates the border between the abdominal coelom and extra-embryonic coelom. The scale bar represents 1 mm. The arrowhead indicates the cecum. The cecum was behind the intestinal loop in HY1. Ad, adrenal gland; CR, colorectum; Du, duodenum; Es, esophagus; In, intestine; Li, liver; Ms, mesonephros; Mt, metanephros; Pa, pancreas; St, stomach; UC, umbilical cord.

Fig. 2 Three-dimensional reconstructed images of the intestinal loop in control 2, HY2, and AG2 embryos. The secondary intestinal loop was confirmed in the extra-embryonic coelom. The red dashed line indicates the border between the abdominal coelom and extra-embryonic coelom. The arrowhead indicates the cecum. The asterisk (*) indicates the end of the intestinal loop in AG2. The scale bar represents 1 mm. CR, colorectum; Du, duodenum; St, stomach.

Fig. 3 Length of the intestinal loop. (A) The blue bar indicates the total digestive tract length (Total length). The red bar indicates the intestinal length within the extra-embryonic coelom (extra length). (B) Ratio of physiological umbilical herniation. The ratio of the intestinal loop length in the extraembryonic coelom (extra length) to the total digestive tract length (Total length).

Fig. 4 Estimated total abdominal cavity volume and intestinal volume. (A) Representative mid-sagittal sectional PXCT images representative of the abdominal cavity in control 1, HY1, and AG1 embryos. The blue line indicates the diaphragm. The red dashed line indicates the border between the abdominal

coelom and extra-embryonic coelom. (B) The estimated total abdominal cavity volume was the sum of the liver volume (Blue bar) and intestinal volume (Red bar). The intestinal volume was estimated as described in Materials and Methods. He, heart; In, intestine; Li, liver; Lu, lung; St, stomach; UC, umbilical cord.

Fig. 5 Representative three-dimensional reconstructed images of the stomach, duodenum, and pancreas in control 1, HY1, and AG1 embryos. The circle indicates the cardia. The square indicates the proximal region of the pancreas connected to the duodenum. The arrow indicates the end of the duodenum, where the duodenum is directly attached to the posterior abdominal wall. The scale bar represents 1 mm. Du; duodenum; Pa, pancreas; SMA, superior mesenteric artery; St, stomach.

Abbreviations

AG = liver agenesis; CS = Carnegie stage; extra length = length of intestinal loop in extraembryonic coelom; HY = liver hypogenesis; PUH = physiological umbilical herniation; PXCT = phase-contrast X-ray computed tomography; Total length = length of total digestive tract

Table 1. Description of liver malformation cases and controls

Case (ID)	CRL	Intestinal length (mm)			Estimated abdominal vol. (mm^3)			Deviation			Other complications	Related figures
	(mm)	TDTL	exL	b/a (%)	Total	Liver	Intestine	Stomach	Duodenum	Pancreas		
control 1 (25858)	19	29	20	69	63	40	24	(-)	(-)	(-)	(-)	F1, F4, F5
control 2 (28066)	18	26	17	65	50	34	16	(-)	(-)	(-)	(-)	F2
HY1 (31528)	21	27	23	84	30	7	23	(-)	(-)	(+)	Gastroschisis (suspicious)	F1, F4, F5 *(SG3)
HY2 (22909)	22	33	22	67	36	8	28	(+)	(+)	(+)	More frequent secondary loops Gastroschisis (suspicious)	F2 *(SG5)
AG1 (31874)	19	23	19	82	21	0	21	(+)	(+)[a]	(+)	(-)	F1,F4, F5 *(SG7)
AG2 (28153)	19	21	18	87	18	0	18	(+)	(+)[a]	(+)	Intestinal atresia between the cecum and colorectum. No right mesonephros and genital ridge.	F2 *(SG6)

CRL, crown rump length; TDTL, total digestive tract length; exL, length of extra-embryonic coelom; b/a, Ratio of exL/TDTL; *, indicate the sample ID described in Kanahashi et al., 2016.

[a] The pyloric antrum to the upper part of the duodenum was straight and ran vertically in the right ventral abdomen.

Fig.1

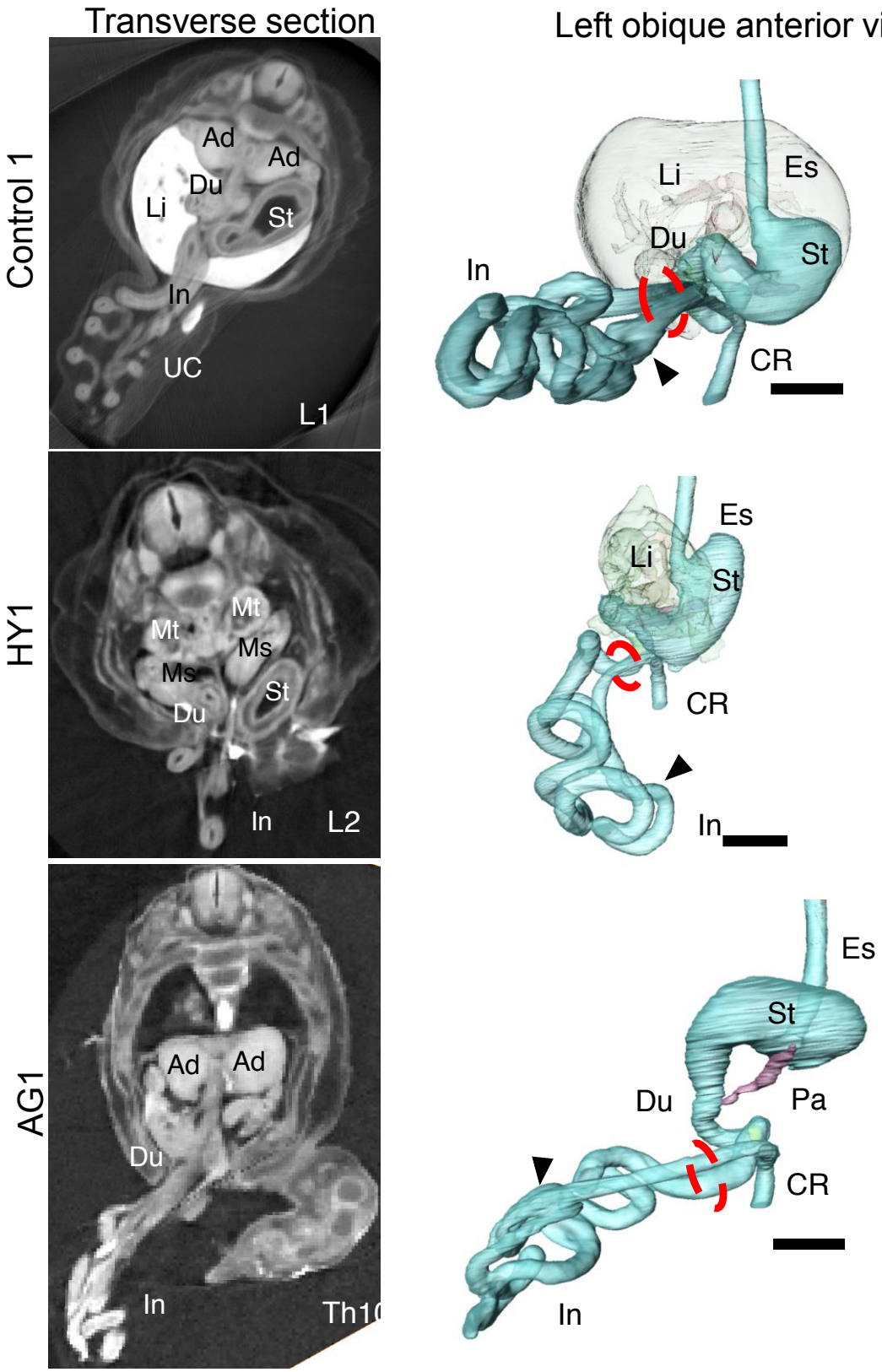

Fig. 1 Three-dimensional (3-D) reconstructed PXCT images and representative 2-D images of control 1, HY1, and AG1 embryos demonstrating physiological umbilical herniation. The red circle indicates the border between the abdominal coelom and extra-embryonic coelom. The scale bar represents 1 mm. The arrowhead indicates the cecum. The cecum was behind the intestinal loop in HY1. Ad, adrenal gland; CR, colorectum; Du, duodenum; Es, esophagus; In, intestine; Li, liver; Ms, mesonephros; Mt, metanephros; Pa, pancreas; St, stomach; UC, umbilical cord.

Fig.2

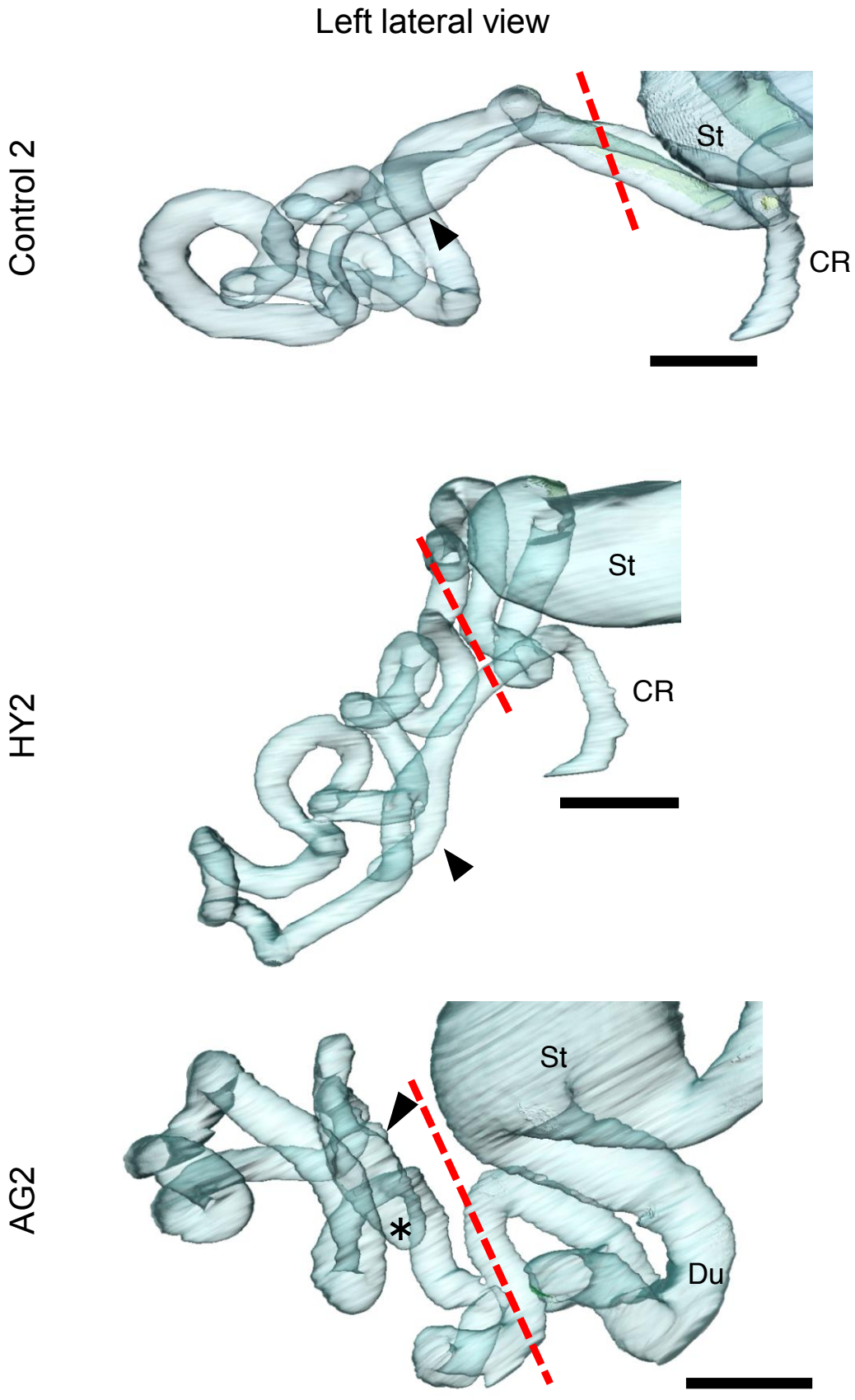

Fig. 2 Three-dimensional reconstructed images of the intestinal loop in control 2, HY2, and AG2 embryos. The secondary intestinal loop was confirmed in the extra-embryonic coelom. The red dashed line indicates the border between the abdominal coelom and extra-embryonic coelom. The arrowhead indicates the cecum. The asterisk (*) indicates the end of the intestinal loop in AG2. The scale bar represents 1 mm. CR, colorectum; Du, duodenum; St, stomach.

Fig.3

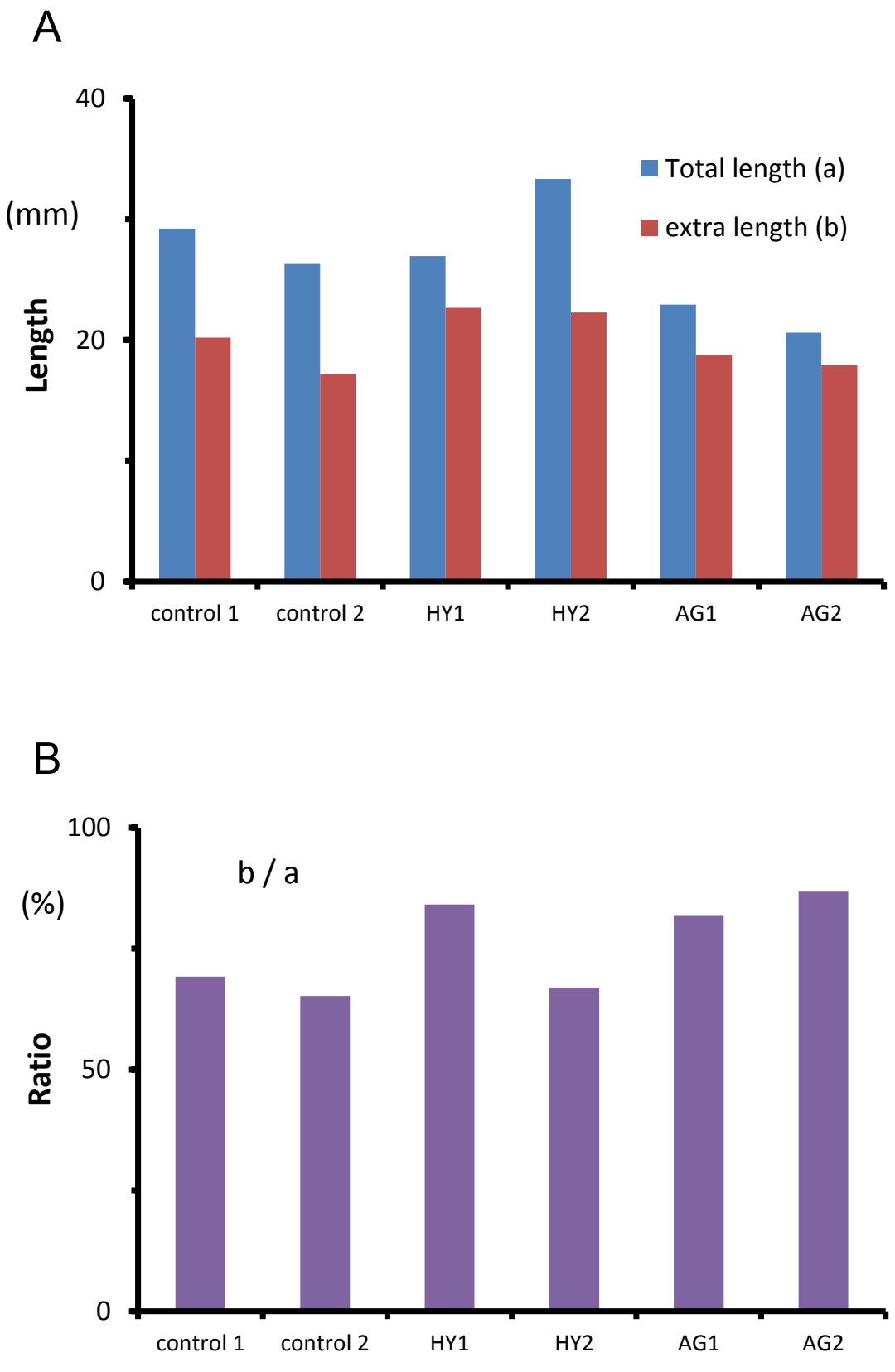

Fig. 3 Length of the intestinal loop. (A) The blue bar indicates the total digestive tract length (Total length). The red bar indicates the intestinal length within the extra-embryonic coelom (extra length). (B) Ratio of physiological umbilical herniation. The ratio of the intestinal loop length in the extraembryonic coelom (extra length) to the total digestive tract length (Total length).

Fig.4

A

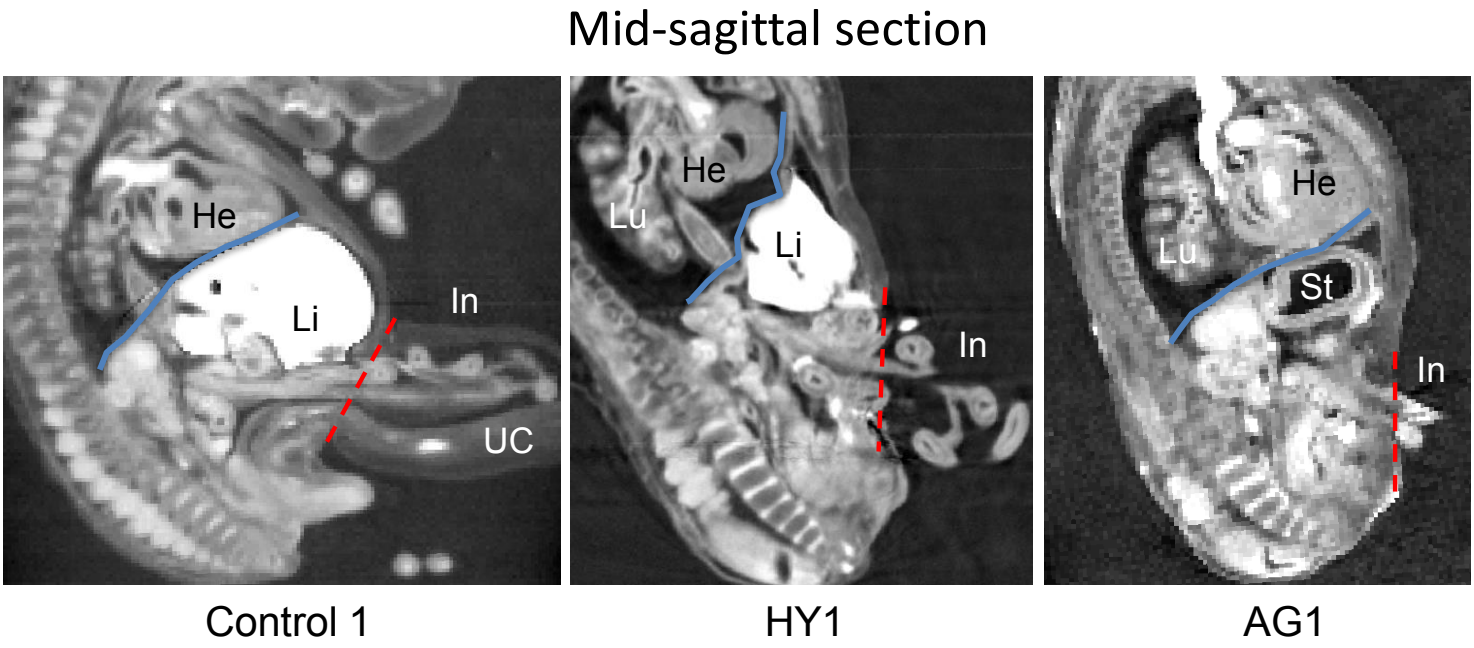

B

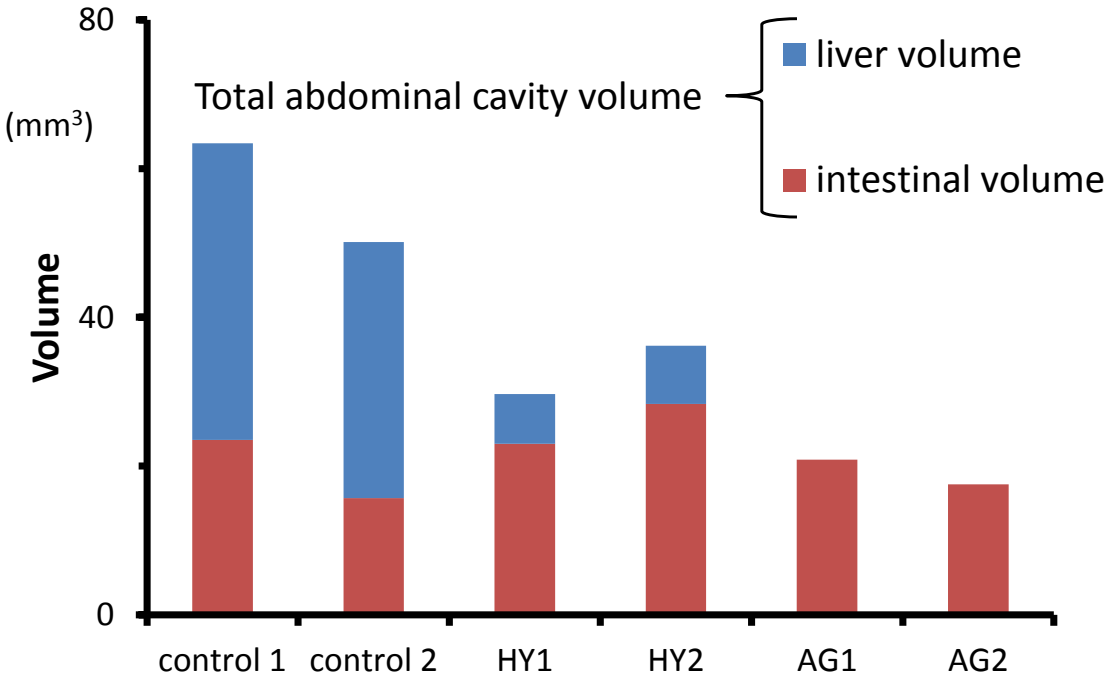

Fig. 4 Estimated total abdominal cavity volume and intestinal volume. (A) Representative mid-sagittal sectional PXCT images representative of the abdominal cavity in control 1, HY1, and AG1 embryos. The blue line indicates the diaphragm. The red dashed line indicates the border between the abdominal coelom and extra-embryonic coelom. (B) The estimated total abdominal cavity volume was the sum of the liver volume (Blue bar) and intestinal volume (Red bar). The intestinal volume was estimated as described in Materials and Methods. He, heart; In, intestine; Li, liver; Lu, lung; St, stomach; UC, umbilical cord.

Fig.5

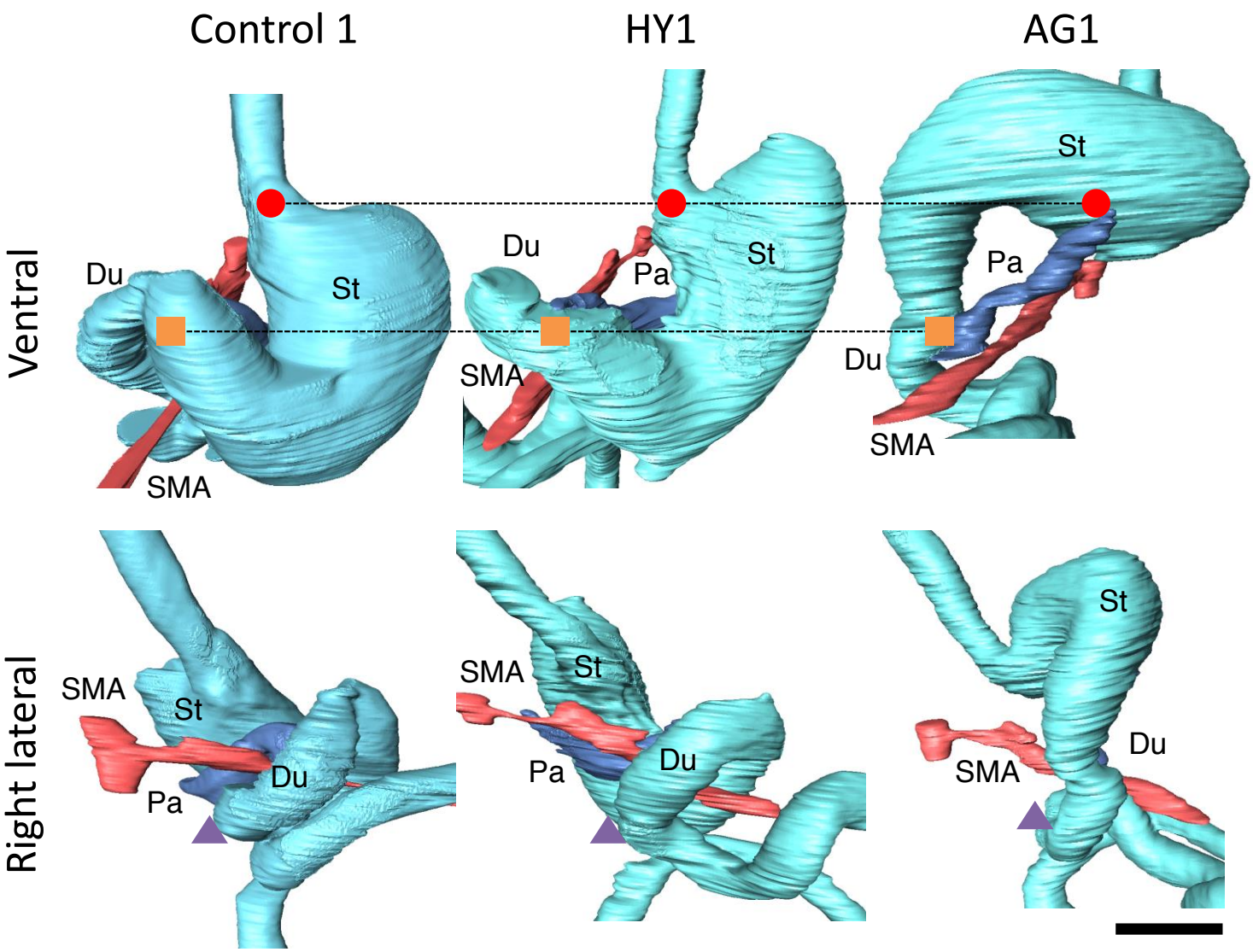

Fig. 5 Representative three-dimensional reconstructed images of the stomach, duodenum, and pancreas in control 1, HY1, and AG1 embryos. The circle indicates the cardia. The square indicates the proximal region of the pancreas connected to the duodenum. The arrow indicates the end of the duodenum, where the duodenum is directly attached to the posterior abdominal wall. The scale bar represents 1 mm. Du; duodenum; Pa, pancreas; SMA, superior mesenteric artery; St, stomach.